



SSC-SDE-17

SSC-SDE
SOLENOIDAL DETECTOR NOTES

MUON (TRIGGER) RATES CALCULATIONS FOR THE SSC DETECTOR

Yoshihide Sakai

Muon (Trigger) Rates Calculations for the SSC Detector

Yoshihide Sakai

KEK, National Laboratory for High Energy Physics
Tsukuba, Ibaraki, Japan 305

ABSTRACT

The muon rates at exit of the calorimeter and the muon filter are calculated using a simple detector geometry for the SSC at $\sqrt{s} = 40$ TeV with $L = 10^{33} \text{cm}^{-2} \text{sec}^{-1}$. Contributions from prompt, decay, and punchthrough are presented as a function of various muon quantities. Also, the efficiencies for typical physics process are calculated for corresponding muon quantities.

INTRODUCTION

At the SSC, many of the new physics signatures involve leptons. Since some of the processes, such as $\text{Higgs} \rightarrow Z^0 Z^0 \rightarrow 4\mu$ and $Z' \rightarrow \mu^+ \mu^-$, involve only muons and no other activities, the muon trigger is quite important (especially at 1st level trigger) to catch those events. Here, the muon rates exiting the calorimeter and the muon filter are calculated for various quantities which might be used in the trigger.

Detector Geometry

In order to calculate the rate of muons, at least the geometry of absorber material should be specified. A simple geometry shown in Fig. 1 is used in the calculation described in the following. A simple cylindrical geometry is assumed: The barrel calorimeter starts from $R = 2$ meters and is treated just as 2 meter thick iron block. A 2.5 meter thick iron muon filter is placed just outside of the calorimeter; The endcap calorimeter starts from $Z = 4$ meters with same thickness of barrel part (2 meter thick iron). A 3.5 meter thick iron muon filter follows it. The inner corner between barrel and endcap corresponds to rapidity $y = 1.5$.

Event Generation

The background events are generated using ISAJET¹ (version 6.21) at $\sqrt{s} = 40$ TeV. In order to estimate background rates in the region relevant to the consideration here (mainly 1st level trigger) including minimum bias events, the process 'TWOJET' in ISAJET are used with wide rapidity range and low p_t limit

for primary jets. The ranges used here are: $-8 < y < 8$ and $5 < p_t < 200 \text{ GeV}/c$. This gives a total cross section of 90 mb which is about same as the expected total cross section ($\sim 100 \text{ mb}$). In order to get enough statistics for full range of consideration, events are generated in 6 steps of p_t ranges.

Muon sources

The following three sources are considered for the muon rate associated with the beam interactions.

i) **Prompt muons:** prompt muons are defined as particle which has muon particle ID in the generated events by ISAJET. These muons come from decays of heavy quarks (c and b). The mass of top quark is set to $160 \text{ GeV}/c^2$ in the program and the contribution to the background muon rate from top quark is negligible in the first level trigger.

ii) **Decay muons:** muons produced by decay in flight of stable hadrons. The decay probability is given by

$$\text{Prob.} = [1 - \exp(-L/c\tau\gamma)] \times \text{Br}(\text{had} \rightarrow \mu x)$$

where L is distance to the surface of calorimeter from the interaction point, $\gamma = E/m_h$, and $\text{Br}(\text{had} \rightarrow \mu x)$ is a branching ratio for muonic decay. Only π^\pm and K^\pm are considered as decay source for simplicity (3-body decay of K_L is neglected). Decay muons coming from two body decay of hadrons with $\beta \sim 1$ have flat energy distribution:

$$E_\mu \cong \gamma(E_\mu^* + p_\mu^* \cos\theta^*), \quad \text{with } -1 < \cos\theta^* < 1$$

iii) **Punchthrough:** There are several empirical parametrization formula which were obtained by fitting experimental data. However, the range of the data in fit is limited and sometimes 2 formula give quite different answers. For example, WA1 parametrization was used in the muon rate calculation at Snowmass 86:²

$$\text{Prob.} = \exp - [(\lambda - 1.53E^{0.33}) / (0.89E^{0.165})]$$

Ref. 3 gives following formula:

$$\text{UA1 Fit : Prob.} = 0.13p^{1.62} \exp(-x/23\text{cm})$$

$$\text{Bodek Fit : Prob.} = (p/350) \times 0.0095 \times \exp[-1.42(\sqrt{R} - 2)] \times 0.81$$

$$\text{Lang Fit : Prob.} = 10^{-4} a \cdot p^b \exp[-(c/p + d)R']$$

(for the detail of formula, see ref. 3). These formula are compared in Fig. 2 for Fe thickness of (a) 2 meters and (b) 4.5 meters. They differ orders of magnitude.

relatively low energy and thin Fe data are used in WA1 and UA1 fits, while relatively high energy and thick Fe data are used in Bodek and Lang fits. In the calculation here, probabilities are calculated both for WA1 and Lang fits and the higher probability is taken for given energy and Fe thickness. This is illustrated in Fig. 3. Basically, WA1 fit is used at thin Fe and Lang fit is used at thick Fe.

Rate calculation

The muon rates are calculated in two ways for decay and punchthrough:

- A) Simulate decay/punchthrough muons according to the calculated probability using random number.
- B) Multiply decay/punchthrough probability as weight for each particle and accumulate histograms for various quantities.

Method A) is more realistic but statistics is much lower than B). Most of the plots shown below is using method B).

RESULTS

The results are presented in terms of the rate (Hz) which is converted from the cross section assuming $L = 10^{33} \text{cm}^{-1} \text{sec}^{-1}$ (i.e. 1 mb corresponds to 10^6 Hz). The overall muon rates for each source are shown in Table 1. The decay muons are dominant source for all cases and the punchthrough gives only small contribution especially after the muon filter.

Table 1. Overall muon rates

y range	Exit at	Prompt(Hz)	Decay(Hz)	Punch(Hz)	Total(Hz)
$ y < 3$	CAL	1.3×10^5	1.1×10^7	5.3×10^5	1.2×10^7
$ y < 3$	Mu Filter	1.1×10^5	5.3×10^5	3×10^3	6.4×10^5
$ y < 1.5$	CAL	1.5×10^4	2.8×10^5	4×10^3	3×10^5
$ y < 1.5$	Mu Filter	2.6×10^3	9×10^3	5×10^1	1.2×10^4

Fig. 4 shows muon multiplicity rates. The rate of multiplicity 2 is an accidental rate of single muons in the same bunch. Therefore, if muon trigger can not separate N bunches the 'dimuon' rate is N times higher. Fig. 5 - 8 show muon rate vs Polar angle and y of muons for each muon source component at the exit of the calorimeter and the muon filter. The rates are presented in two plots for each case: a) The (differential) rate at given quantity value; b) The trigger rate with given threshold value for the quantity. This is given by integrating the differential rate a) from threshold value to infinite. In order to minimize statisti-

cal effect, the integration was done after smoothing the distribution shown in a). The values at the lowest point gives total rate. Fig. 9 - 12 show muon rate vs p_t and p for rapidity range $|y| < 3$ and Fig. 13 - 16 shows those for $|y| < 1.5$. For p_t and p plots, momenta of decay muons are used rather than momenta of parent hadrons, since momenta measured by the muon detector would be relevant to the muon triggers for early stage. For punchthrough muons, momenta of hadron are used for convenience. Fig. 17 compares the total muon rates vs p_t/p threshold values for various cases.

Most of new physics signatures give leptons to be isolated. A simple isolation algorithm is considered here. The calorimeter energy deposit around muon track are checked for single, 9 (3×3), and 25 (5×5) calorimeter towers. The calorimeter energy deposit is simulated using simple calorimeter simulation program CALSIM⁴ with tower size $\Delta y \times \Delta \phi = 0.15 \times 2\pi/32$. Fig. 18 (a),(b) show energy deposit distributions of the calorimeter towers. Fig. 19 show trigger rate versus calorimeter isolation energy threshold E_{CAL} where if calorimeter towers have energy deposit more than E_{CAL} , the events are rejected. It shows rate does not decrease so much. Probably, without muon momentum cut, majority of muon rates are due to low momentum particles and already away from the hard component of the jet.

Efficiency for Physics Events

For any quantity, the trigger rate can be reduced to any value by raising the threshold. However, the threshold should be kept low enough to keep the efficiency of the interesting physics events to be good enough. As an example, the Higgs production process ($H \rightarrow W^+W^- \rightarrow \mu + \nu + \text{jets}$) is chosen. The mass of Higgs is chosen to be $400 \text{ GeV}/c^2$. The events are generated using ISAJET program. The total cross section of the process is 0.46 pb including branching ratios.

The results are shown in Fig. 20-23. Now a) shows the differential cross section and b) shows the efficiency vs threshold value for each set.

From the background distributions, it is important to have p_t or p threshold in the first level trigger in order to reduce the muon trigger rate to comfortable level. p_t (or p) threshold of 20 (40) GeV/c is enough to reduce background rates to the level of 10^3 , while the efficiency for Higgs production process still kept more than 80%.

The author wishes to thank Dr. Y.Takaiwa for providing ISAJET program package and help and discussions for proceeding the calculations. He also wishes to express his thanks to Prof. Y.Watase for giving opportunity to participate series of related workshops and his encouragement throughout of this work.

REFERENCES

- 1) F.E.Paige and S.D.Protopopescu, BNL-37066 (1985).
- 2) "SSC Muon Detector Group Report", page 405 in Snowmass 1986 Proceedings.
- 3) A.Bodek, UR911 ER13065-412 (1985).
- 4) F.E.Paige, Proceedings of the Workshop on Triggering, Data Acquisition and Computing for the High Energy/High Luminosity Hadron - Hadron colliders, Fermilab (1985), Page 51.

FIGURE CAPTIONS

- Fig. 1. Geometry used in the calculation.
- Fig. 2. Comparison of punchthrough probability given by different parametrizations for iron thickness of (a) 2 meters and (b) 4.5 meters.
- Fig. 3. illustration of punchthrough probability use in the calculation.
- Fig. 4. Muon multiplicity rate at exit of calorimeter and muon filter.
- Fig. 5. Muon rate vs polar angle of muons at exit of calorimeter.
- Fig. 6. Muon rate vs polar angle of muons at exit of muon filter.
- Fig. 7. Muon rate vs rapidity of muons at exit of calorimeter.
- Fig. 8. Muon rate vs rapidity of muons at exit of muon filter.
- Fig. 9. Muon rate vs p_t of muons at exit of calorimeter for $|y| < 3$.
- Fig. 10. Muon rate vs p_t of muons at exit of muon filter. for $|y| < 3$.
- Fig. 11. Muon rate vs p of muons at exit of calorimeter for $|y| < 3$.
- Fig. 12. Muon rate vs p of muons at exit of muon filter. for $|y| < 3$.
- Fig. 13. Muon rate vs p_t of muons at exit of calorimeter for $|y| < 1.5$.
- Fig. 14. Muon rate vs p_t of muons at exit of muon filter. for $|y| < 1.5$.
- Fig. 15. Muon rate vs p of muons at exit of calorimeter for $|y| < 1.5$.
- Fig. 16. Muon rate vs p of muons at exit of muon filter. for $|y| < 1.5$.
- Fig. 17. Comparison of total muon rate vs (a) p_t and (b) p of muons for: at exit of calorimeter and muon filter; and $|y| < 3$ and 1.5.
- Fig. 18. Distribution of energy deposit corresponding muon position with single, 9, and 25 calorimeter towers for muons exiting calorimeter (a) and exiting muon filter (b).
- Fig. 19. Rate vs E_{CAL} for isolation requirement for rapidity range $|y| < 3$ (a) and $|y| < 1.5$ (b).
- Fig. 20. Muon rate vs polar angle of muons at exit of muon filter for Higgs production: $H(400 \text{ GeV}) \rightarrow W^+W^- \rightarrow \mu + \nu + \text{jets}$.
- Fig. 21. Muon rate vs p_t of muons at exit of muon filter for Higgs production: $H(400 \text{ GeV}) \rightarrow W^+W^- \rightarrow \mu + \nu + \text{jets}$.
- Fig. 22. Muon rate vs p of muons at exit of muon filter for Higgs production: $H(400 \text{ GeV}) \rightarrow W^+W^- \rightarrow \mu + \nu + \text{jets}$.
- Fig. 23. (a) Distribution of energy deposit corresponding muon position with single, 9, and 25 calorimeter towers for muons exiting muon filter with $|y| < 3$ for Higgs production: $H(400 \text{ GeV}) \rightarrow W^+W^- \rightarrow \mu + \nu + \text{jets}$. (b) Rate vs E_{CAL} for isolation requirement for (a).

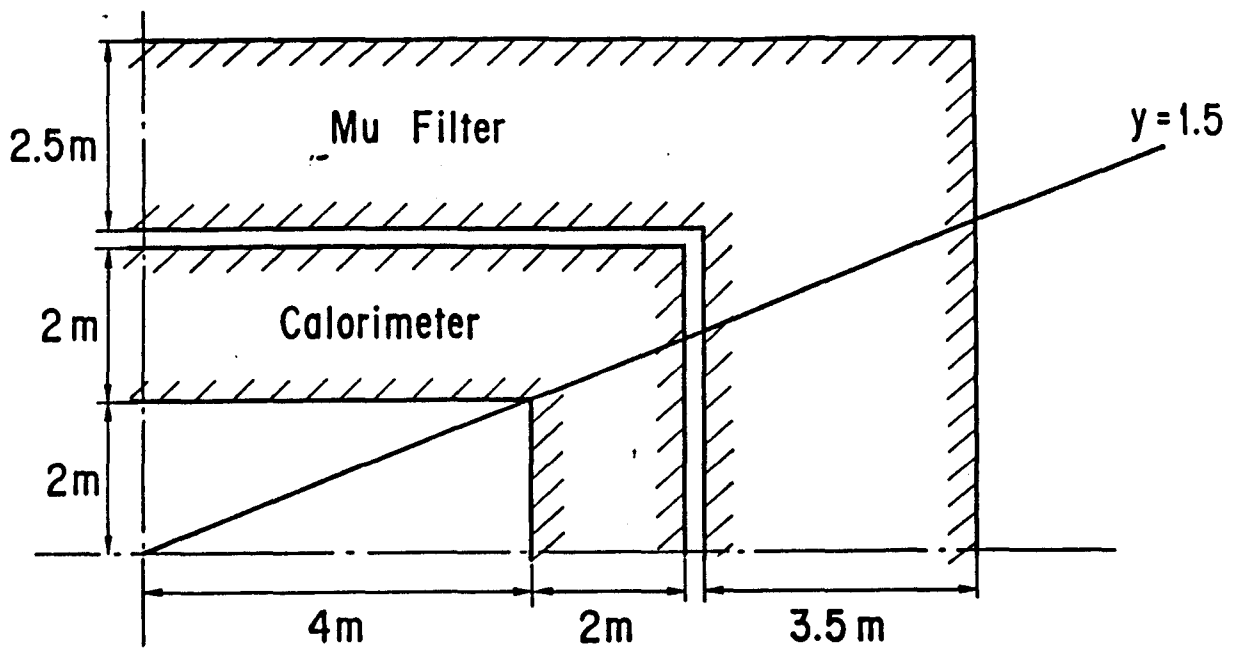


Fig. 1

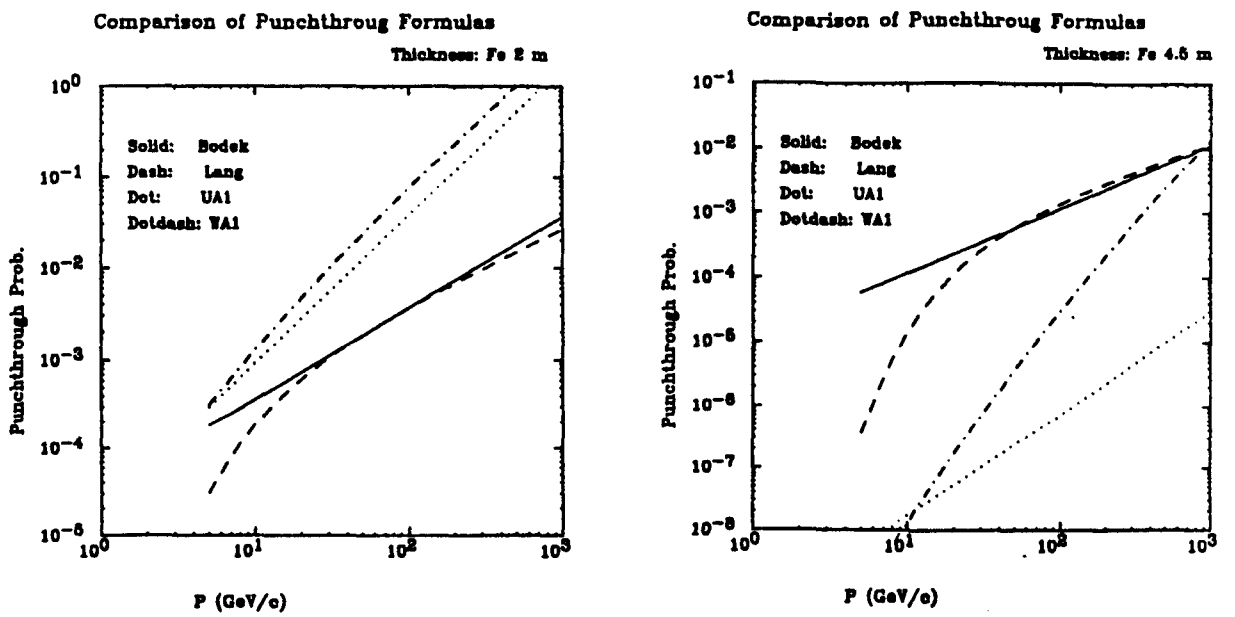


Fig. 2

Comparison of Punchthrough Formulas

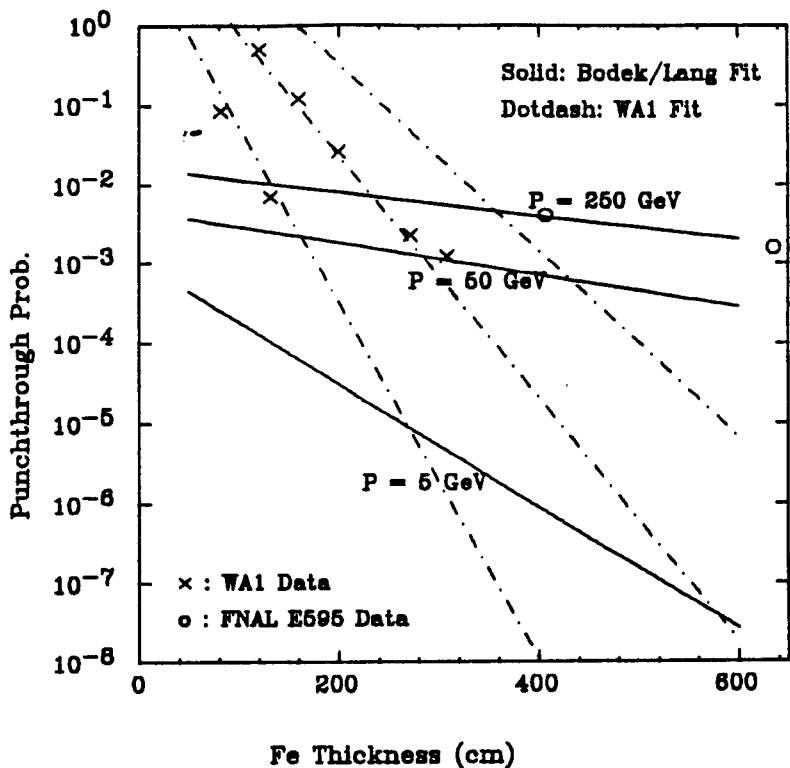


Fig. 3

Muon Multiplicity Rate

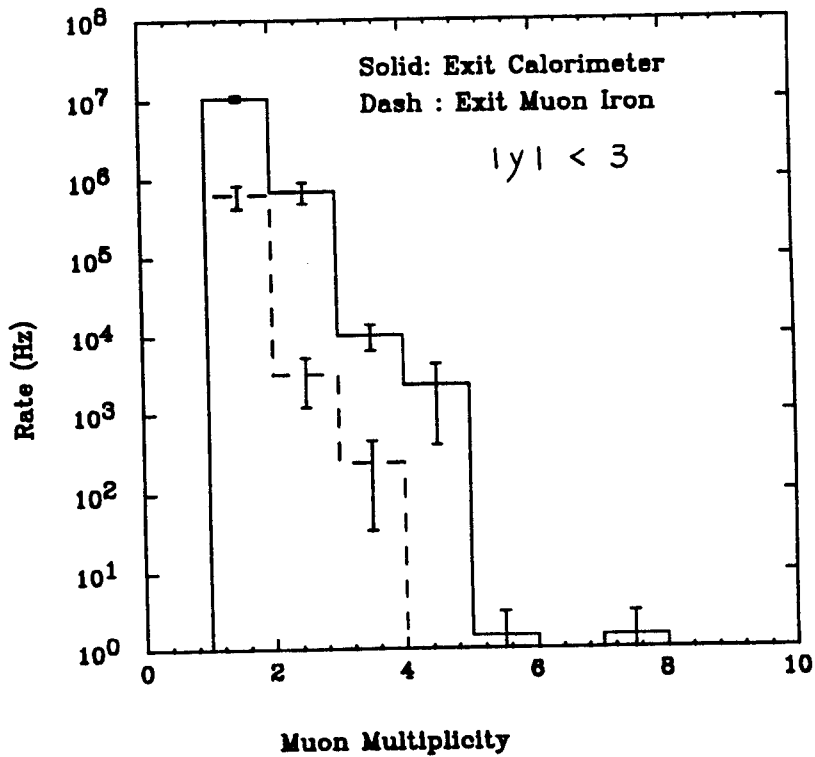
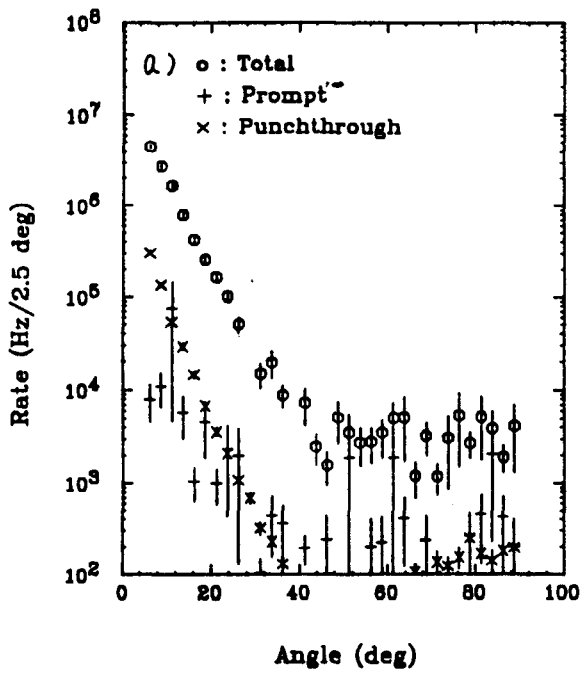


Fig. 4

Muon Rate vs Polar Angle



Exit Calorimeter

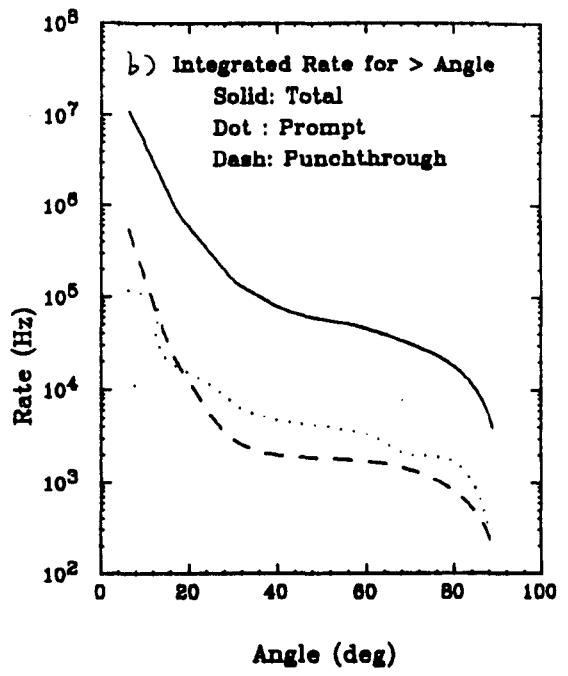
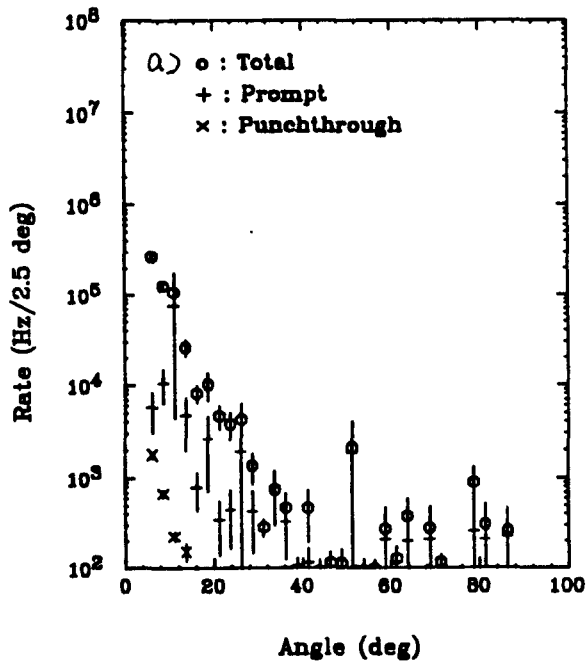


Fig. 5

Muon Rate vs Polar Angle



Exit Muon Iron

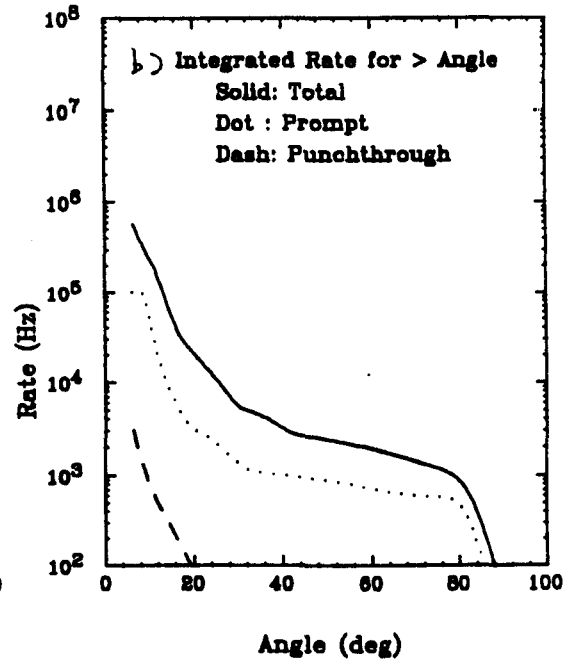
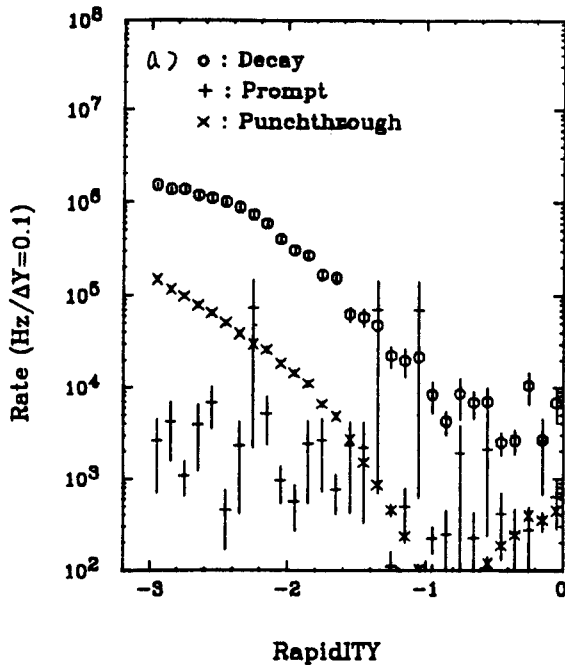


Fig. 6

Muon Rate vs Rapidity



Exit Calorimeter

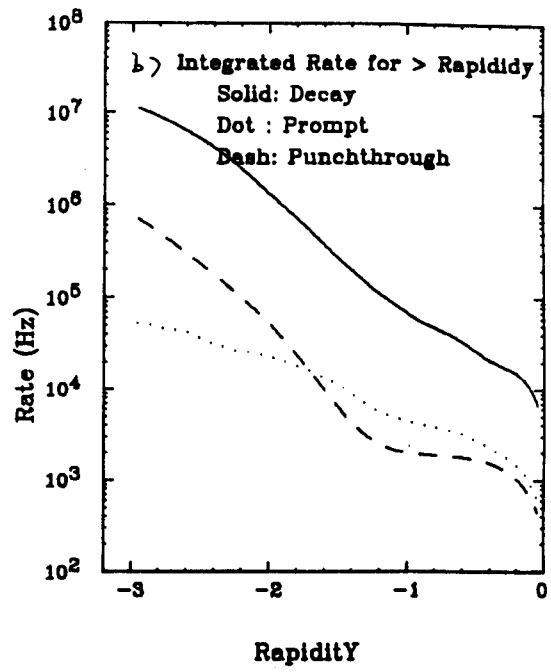
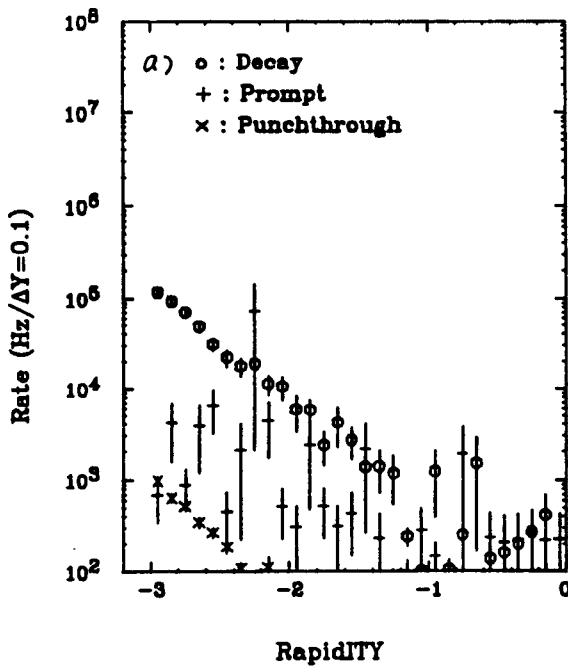


Fig. 7

Muon Rate vs Rapidity



Exit Muon iron

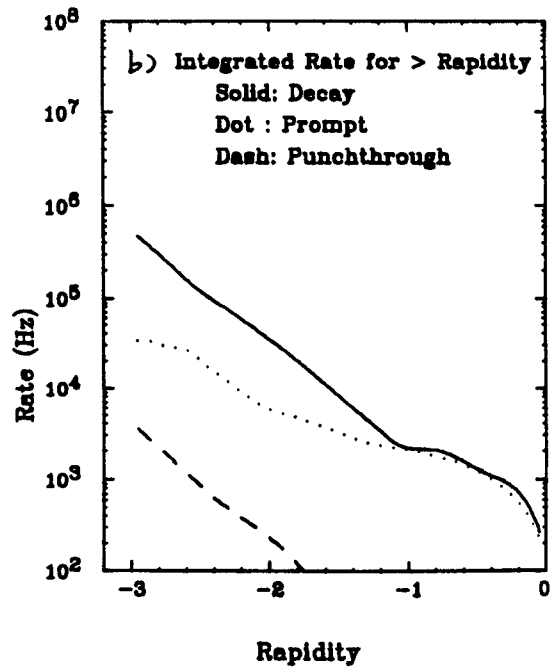


Fig. 8

Muon Rate vs PT of Muons

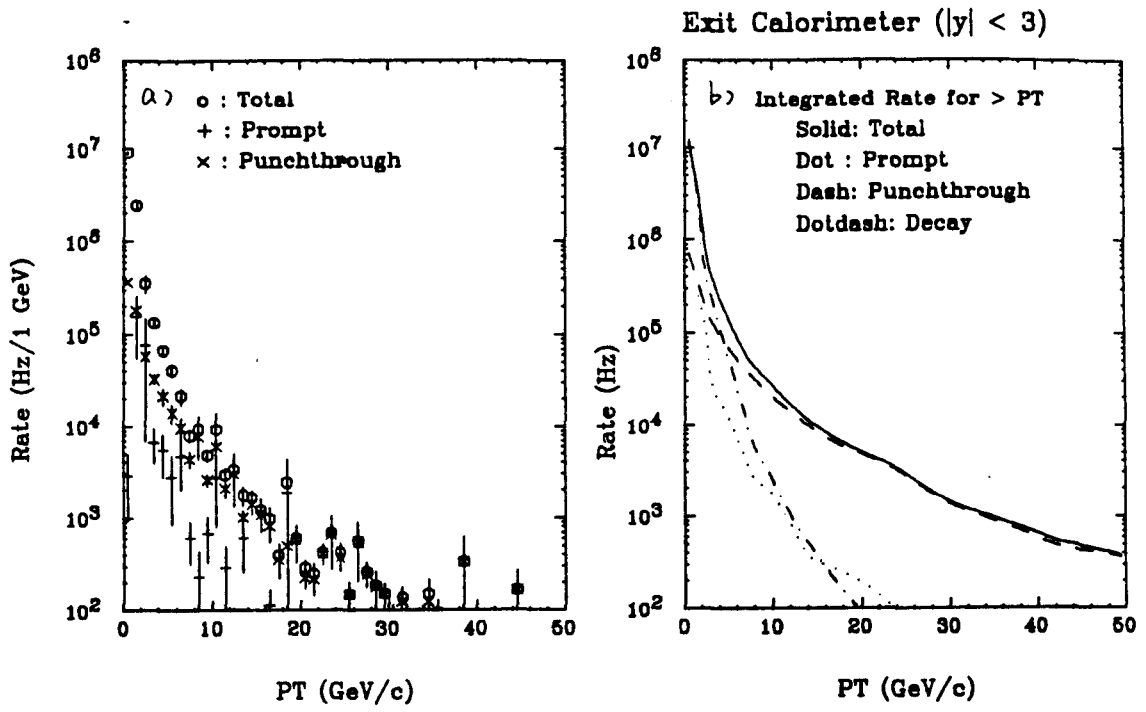


Fig. 9

Muon Rate vs PT of Muons

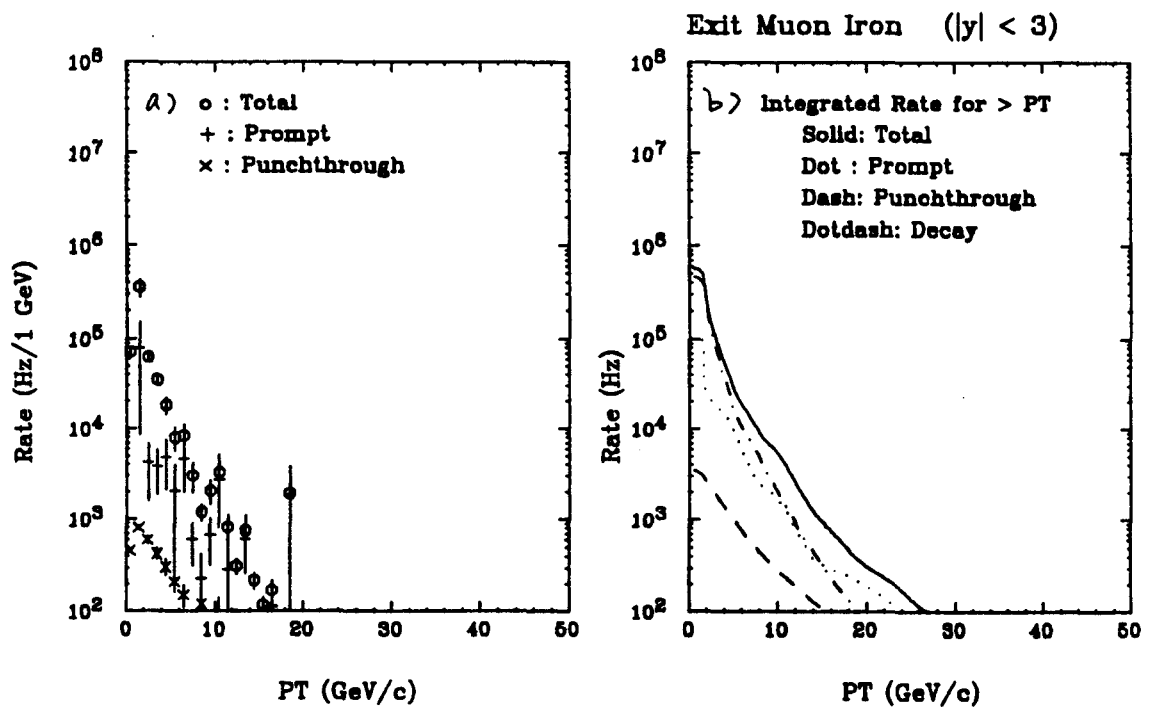


Fig. 10

Muon Rate vs Muon Momentum

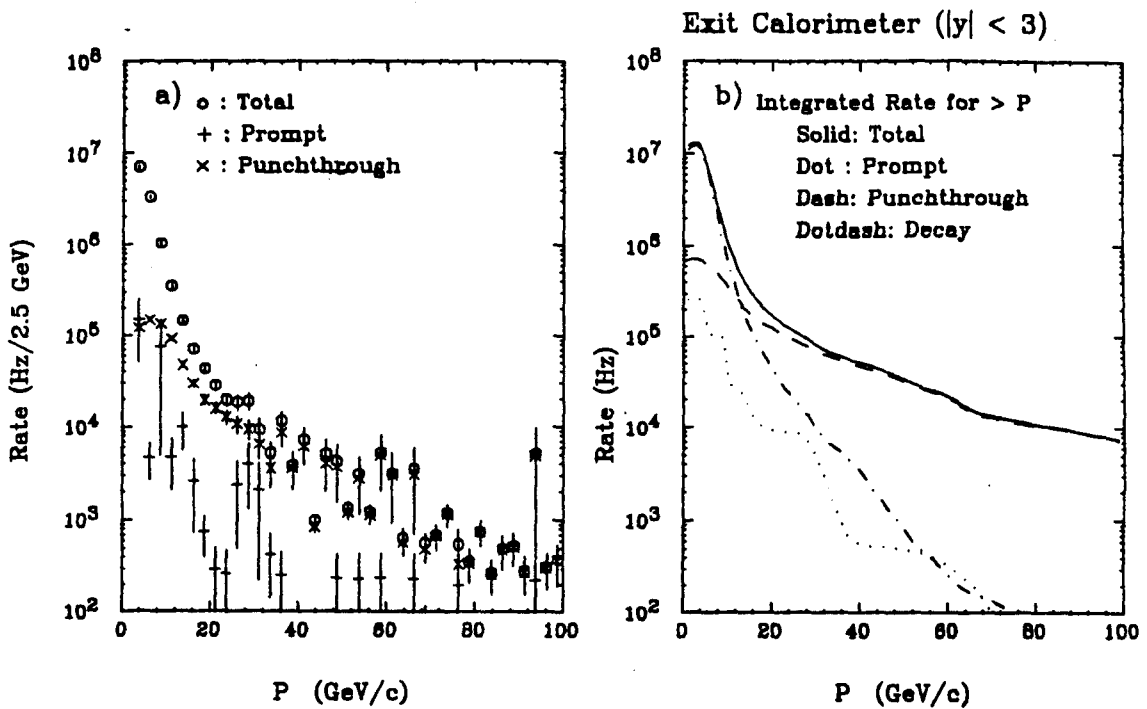


Fig. 11

Muon Rate vs Muon Momentum

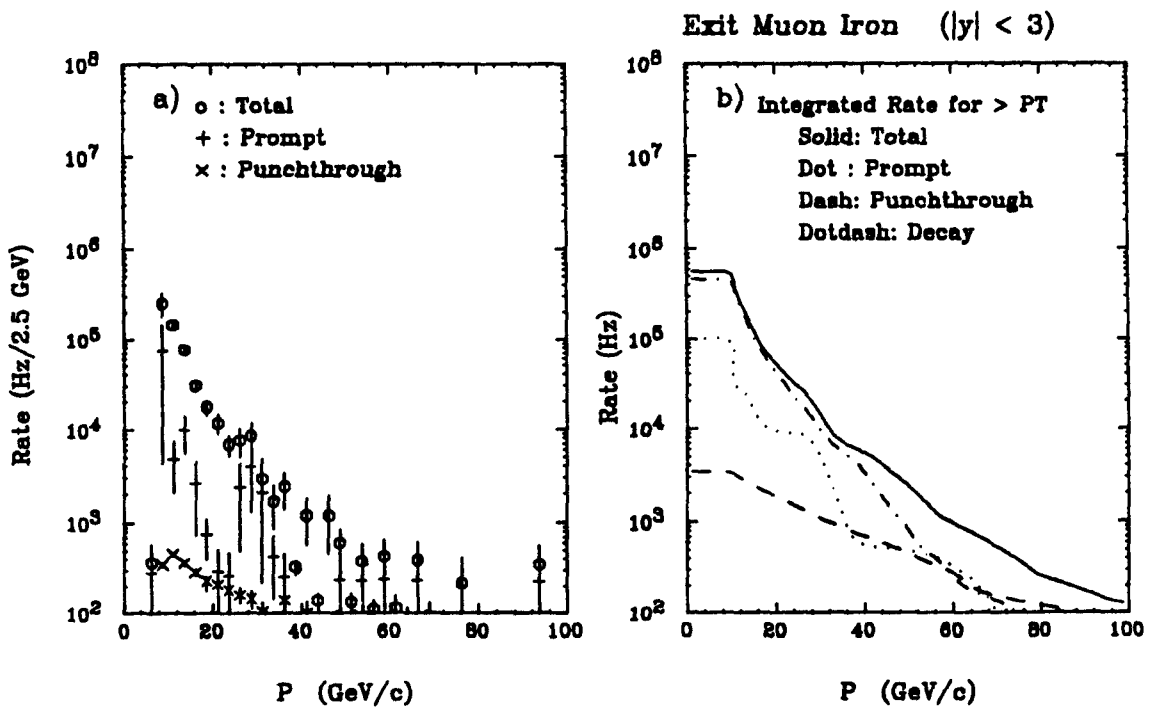


Fig. 12

Muon Rate vs PT of Muons

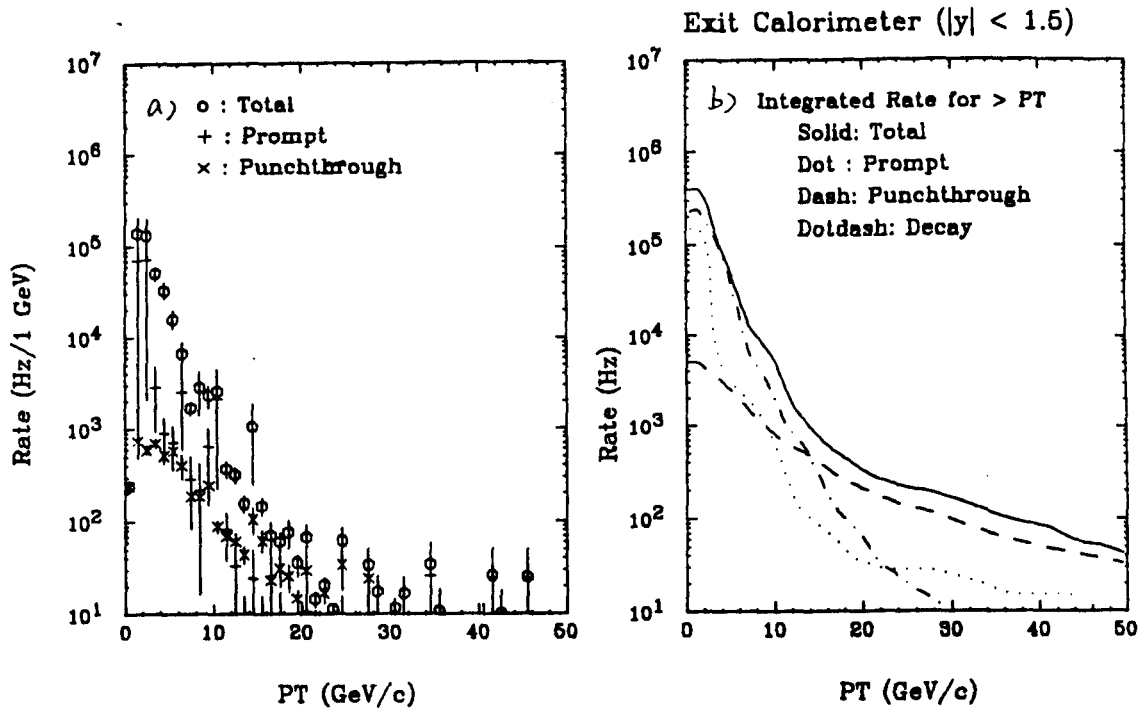


Fig. 13

Muon Rate vs PT of Muons

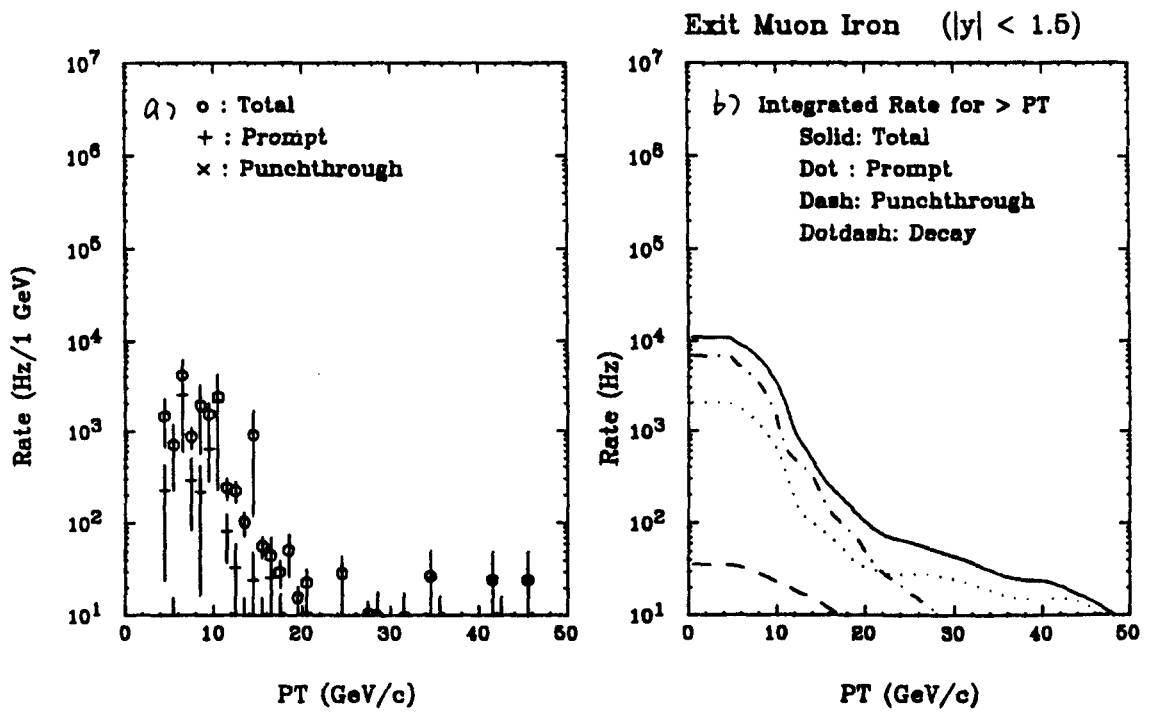


Fig. 14

Muon Rate vs Muon Momentum

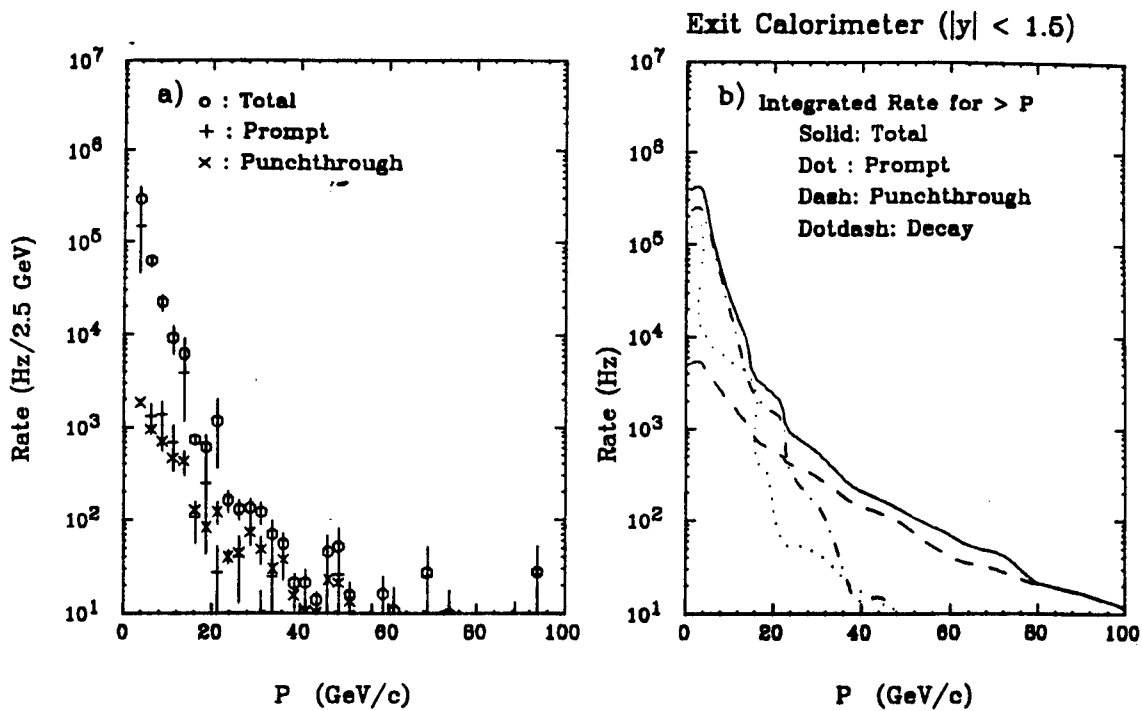


Fig. 15

Muon Rate vs Muon Momentum

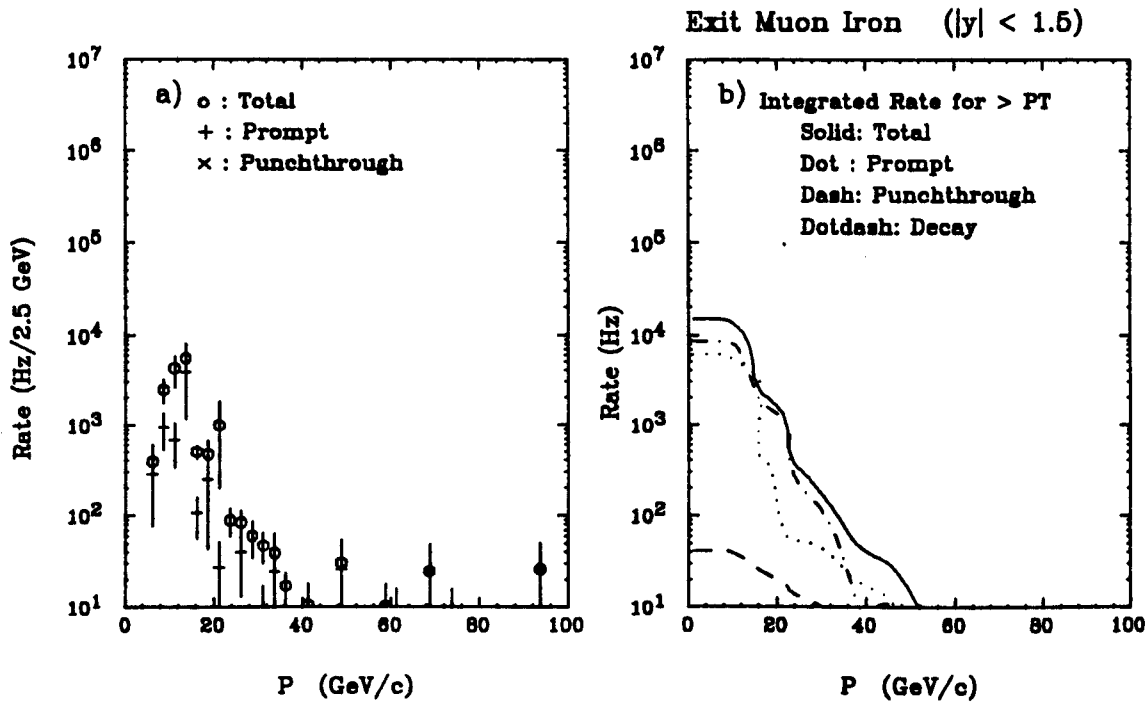


Fig. 16

Muon Rate vs PT/P Threshold

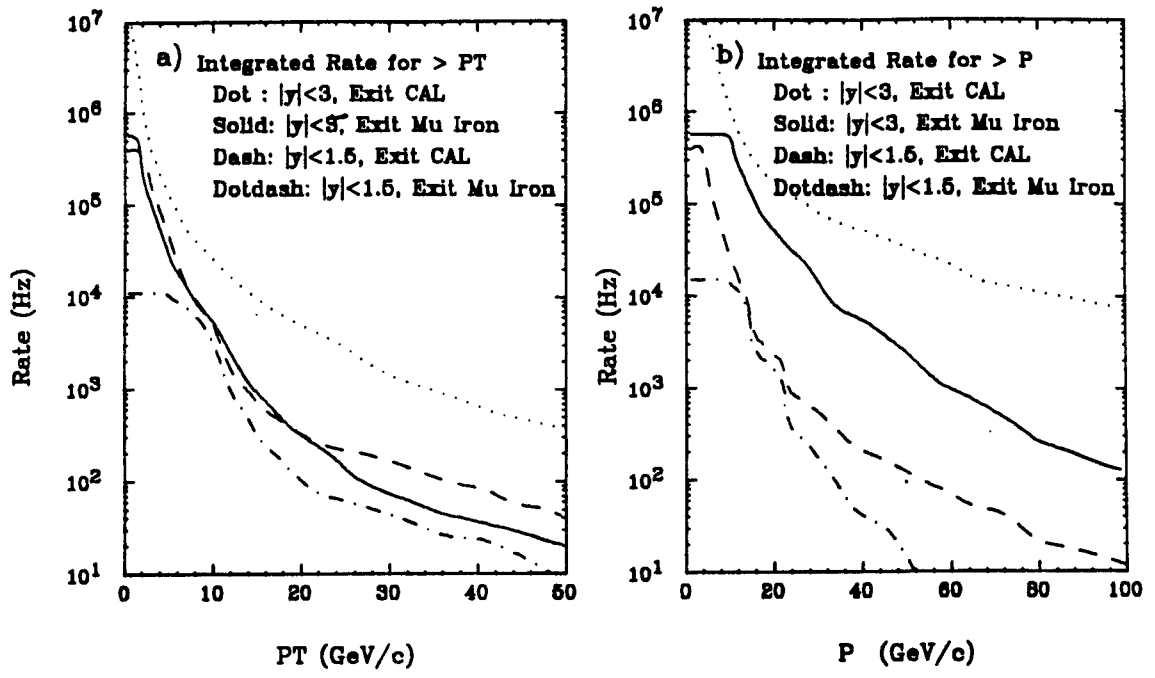


Fig. 17

Muon Rate vs Isolation

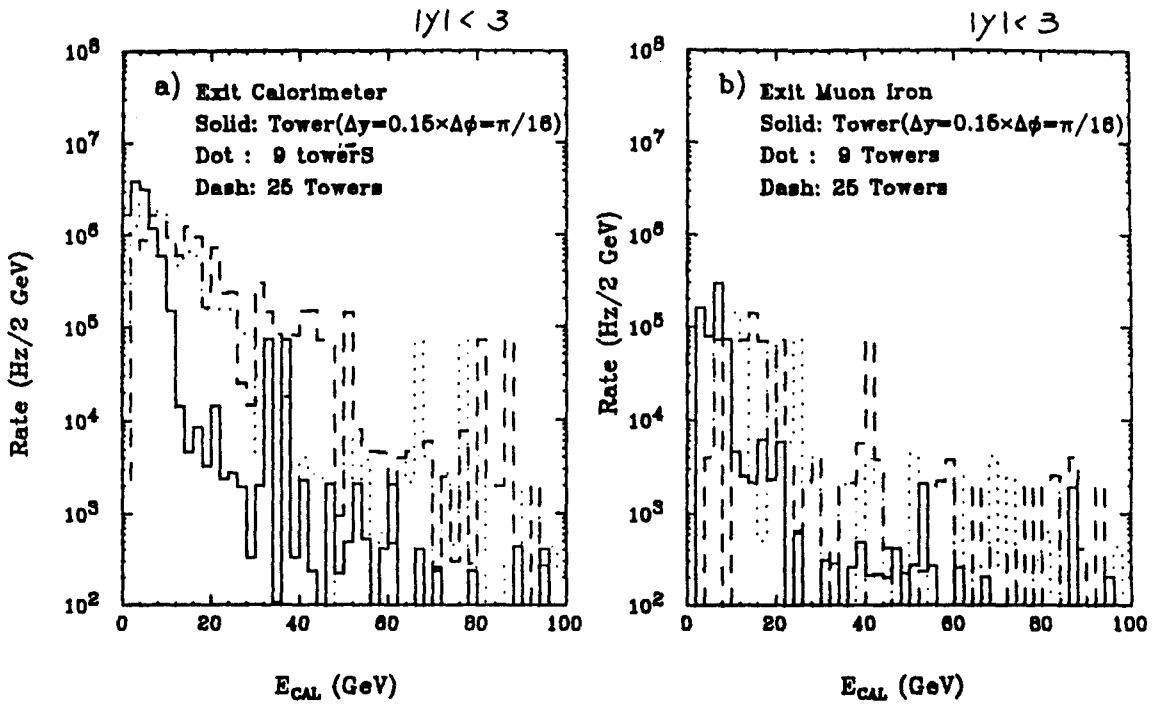
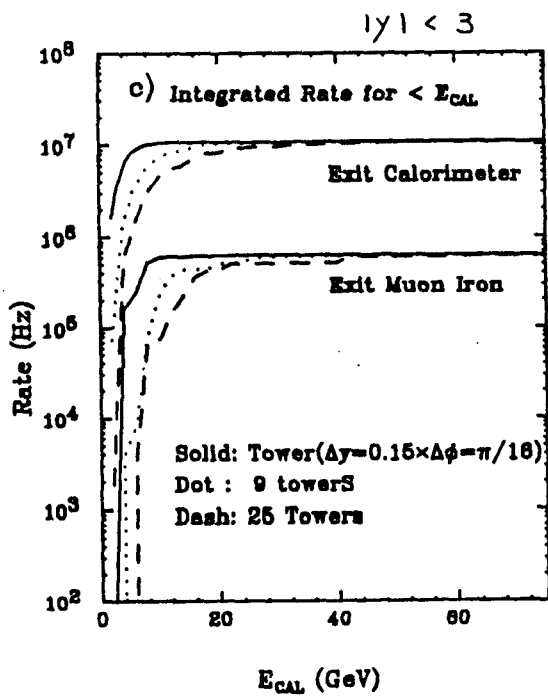


Fig. 18

Muon Rate vs Isolation



Muon Rate vs Isolation

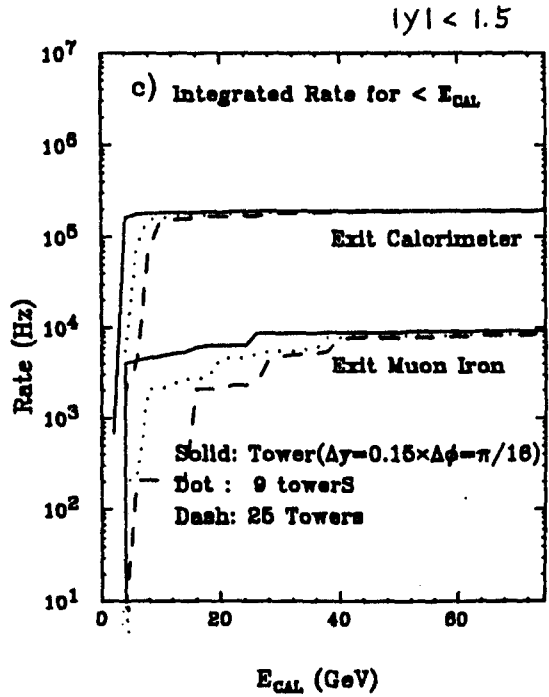


Fig. 19

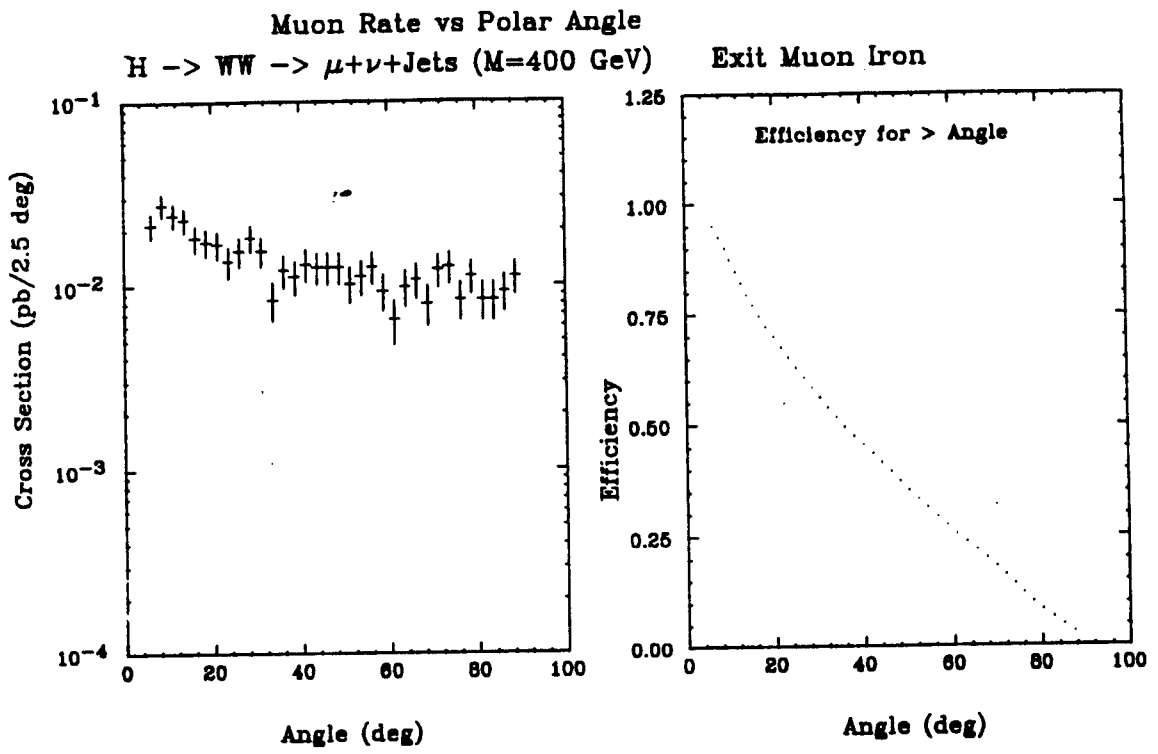


Fig. 20

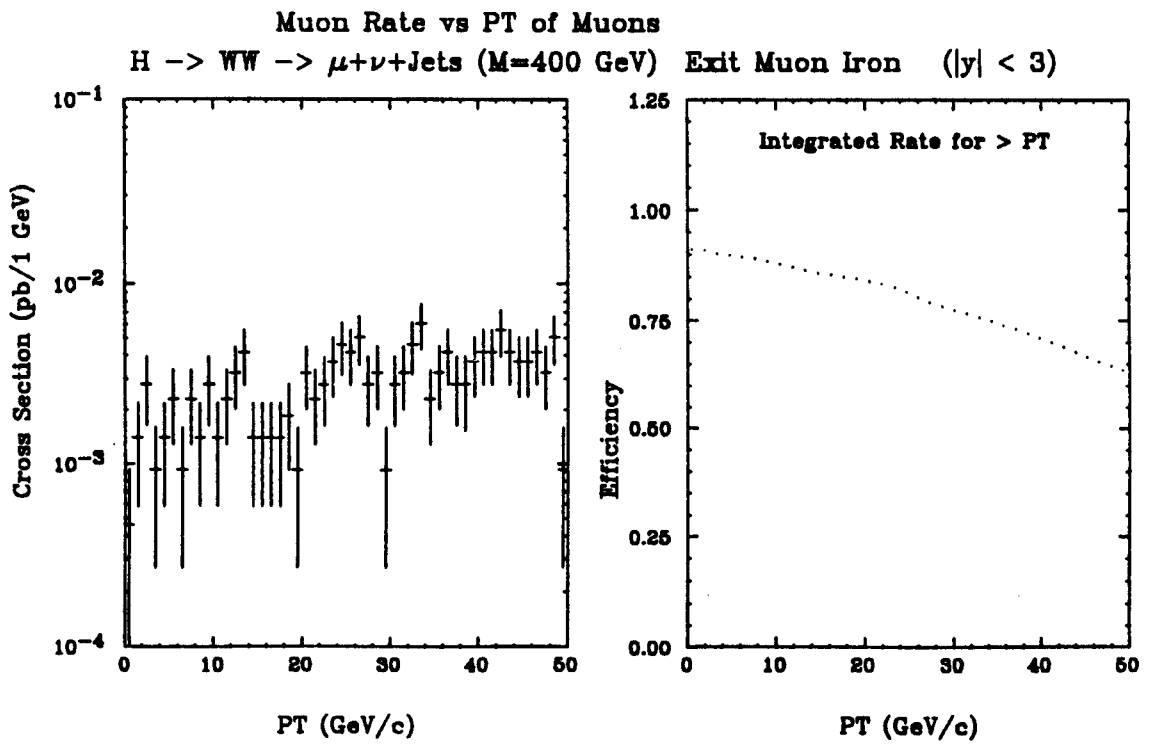


Fig. 21

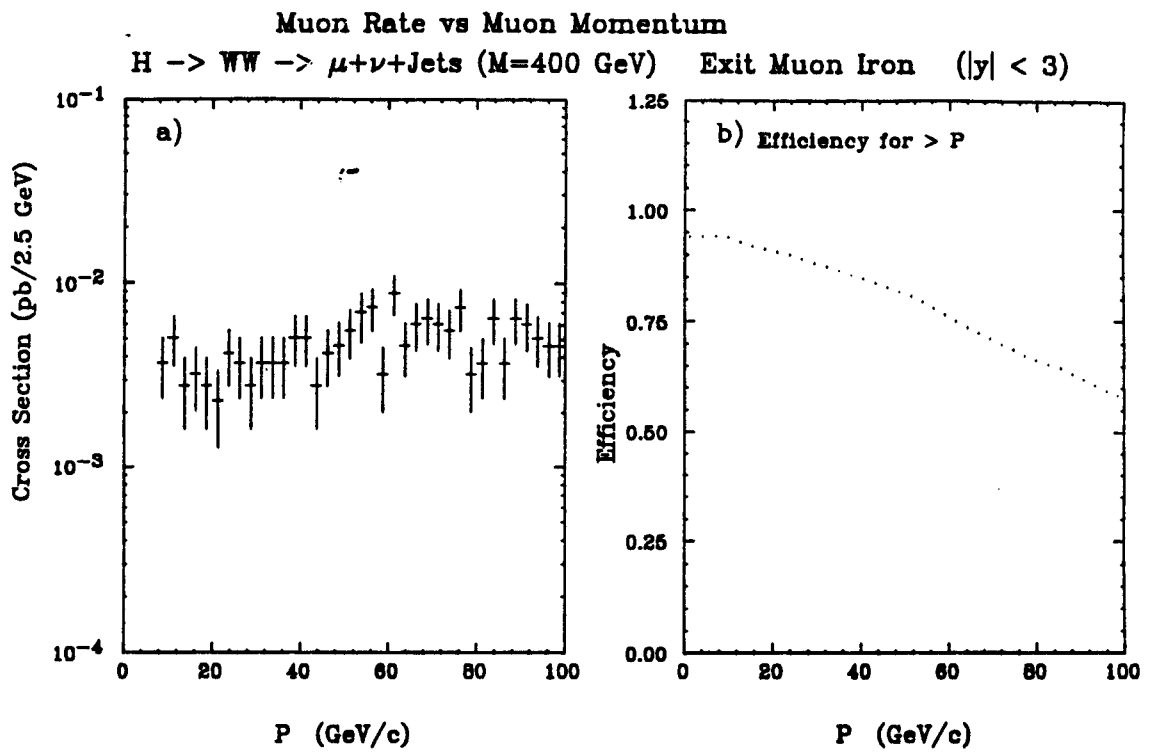


Fig. 22

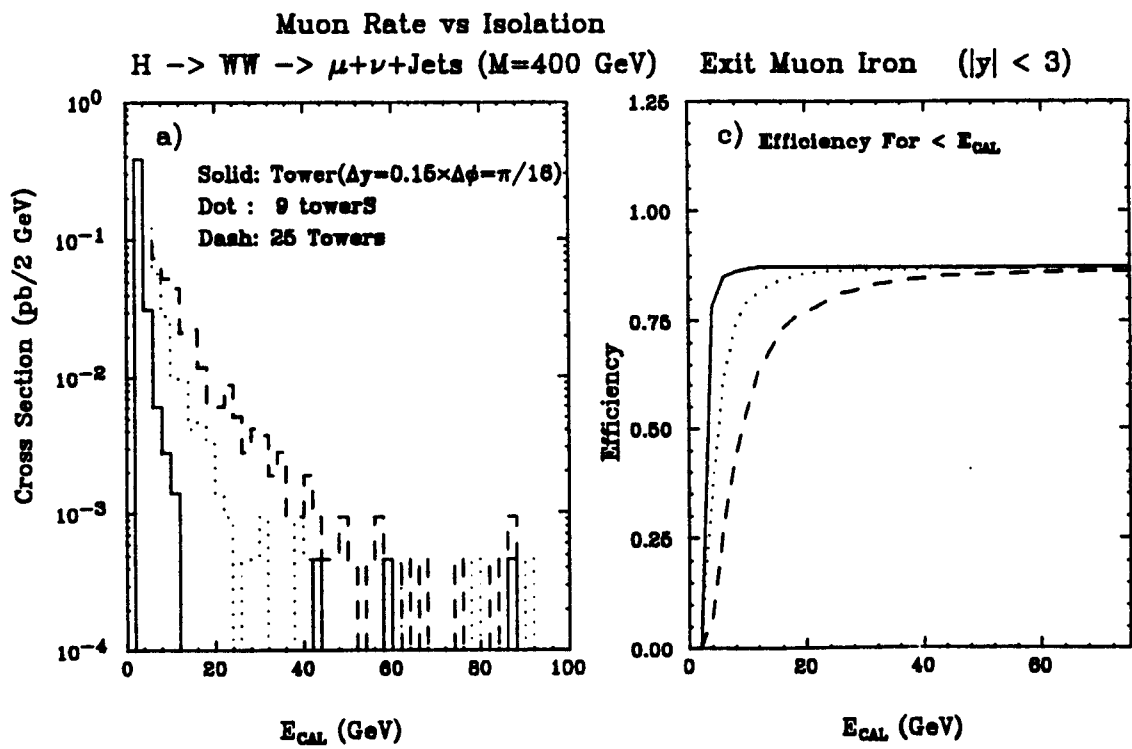


Fig. 23